Electronic Supplementary Material (ESI) for Journal of Materials Chemistry A.

Supporting information

Self-Assembled CuS-MXene Bridge for Hole-Boosting 10.51%-Efficiency All-Inorganic Tri-Brominated Perovskite Solar Cells

Weilin Liu,[#a] Xinpeng Yao,[#a] Benlin He,*[a] Haojie Sui,[a] Meng Wei,[a] Haiyan Chen,[a] Jialong Duan[b] and Qunwei Tang*[b]

[a] School of Materials Science and Engineering, Ocean University of China, Qingdao 266100, PR China

[b] Institute of Carbon Neutrality, College of Chemical and Biological Engineering, Shandong University of Science and Technology, Qingdao 266590, PR China

*** Corresponding Author.** E-mail: blhe@ouc.edu.cn, tangqunwei@jnu.edu.cn

Experimental Section

Materials: Stannous Chloride Anhydrous ($SnCl_2$, ≥99.0%), Thiourea (CH_4N_2S, ≥99.0%), Acetamide Sulfide (C_2H_5NS, ≥99.0%) Lead bromide ($PbBr_2$, ≥99.0%) and Cesium bromide (CsBr, ≥99.9%) were all brought from Aladdin Industrial Corporation. Titanium Aluminum Carbide (Ti_3AlC_2, ≥98%, 200 meshes) was purchased from Jilin 11 technology Co., Ltd. Hydrofluoric acid (HF, ≥40%), Copper chloride dihydrate ($CuCl_2 \cdot 2H_2O$, ≥99.9%), Ethylene glycol ($C_2O_2H_6$, AR) and Isopropanol (C_3H_8O, AR) were all brought from Sinopharm Chemical Reagent Co., Ltd. All materials and reagents were used directly without purification.

Preparation of MXene ($Ti_3C_2T_x$): 1 g of Ti_3AlC_2 powder was slowly added into 20 mL of HF solution (40%) and stirred at 35 °C for 24 h. Then the etched colloidal solution was centrifuged with deionized water (3500 rpm, 5 min) for several times until pH>5 and sonicated in an ice bath for 2 h under the protection of inert atmosphere. A dark green supernatant was obtained from the above solution after centrifugation (6000 rpm) for 1 h and freeze-dried to prepare the two-dimensional slice of MXene with single or few layers.

Preparation of CuS-MXene and CuS: Firstly, 0.2 g of MXene powder was dispersed in 60 mL of ethylene glycol and then 40 mg of $CuCl_2 \cdot 2H_2O$ was slowly added and magnetically stirred for 30 min. Then 40 mg of thioacetamide (TAA) was slowly added and stirred for 30 min. The mixed solution was poured into a hydrothermal kettle and heated at 150 °C for 9 h. After hydrothermal treatment, the solution was centrifuged with ethanol and deionized water (3500 rpm, 5 min) by turn and freeze-dried to obtain the CuS-MXene powder. The CuS powder was prepared under the same conditions without adding MXene.

Device fabrication: All experimental processes were conducted in air without any additional condition control. Firstly, the conductive glass of FTO was etched with Zn powder and HCl (2 M), and then ultrasonically cleaned with deionized water and anhydrous ethanol in turn. The washed FTO substrate was treated in plasma equipment for 400 seconds and preheated on a 90 °C heating plate for 3 min. The SnO_2 QDs solution prepared by low-temperature solution technology[1] was also preheated on a 90 °C heating plate for 3 min and spin-coated on the FTO substrate for 30 s at the speed of 2000 rpm, and annealed at 200 °C for 60 min to obtain a dense SnO_2 layer. Next, the N, N-dimethyl formamide (DMF) solution of 1 M $PbBr_2$ was spin-coated on the SnO_2 substrate (2000 rpm, 30 s) and heated at 80 °C for 30 min. After that, the methanol solution of 0.07 M CsBr was spin-coated (2000 rpm, 30 s) and annealed at 250 °C for 5 min. The above step was repeated seven times to prepare a high quality $CsPbBr_3$ film. Subsequently, the isopropanol solution of MXene or CuS-MXene (2 mg mL^{-1}) was spin-coated on the perovskite film and annealed at 100 °C for 5 min. At last, a conductive carbon paste was blade coated onto the MXene or CuS-MXene layer and treated at 90 °C for 30 min to obtain a complete PSC with an active area of 0.09 cm^2.

Measurements and characterizations: XPS was obtained by using the PHI-5000CESCA system (Perkin Elmer) with Mg Kα radiation. Field emission scanning electron microscope (SEM, S4800, Hitachi) was used to characterize the surface images of various films, cross-section image of the whole device and energy dispersive spectroscopy (EDS) mapping images of MXene or CuS-MXene powder. The TEM images were taken on JEM 2100 LaB6 at 200 kV. The HRTEM was all operated on Tecnai F20 at 200 kV. XRD characterization was performed on

a PHILIPSPW1800 diffractometer (Cu-Kα radiation). UV-vis transmission and absorption spectra were characterized using Meipuda UV-3200 spectrophotometer. The zeta potential of various samples was measured by the Brookhaven 90 Plus/PALS instrument. The image of atomic force microscopy (AFM) was performed with an Innova Scanning Probe Microscope 9700 (Shimadzu, Japan). The UPS tests were carried out through a Kratos AXIS ULTRA system. A space charge limited current (SCLC) model was employed to characterize the trap density of perovskite films for hole-only equipment with the structure of FTO/NiO/$CsPbBr_3$/MXene or CuS-MXene/Carbon in the voltage range of 0-7 V under dark conditions. The PL and TRPL spectra were detected by the FLS920 and Horiba spectrofluorometer, respectively. The *J-V* curves of various devices were measured by the sourcemeter of Keithley 2400 under irradiation of simulated sunlight (AM 1.5G, 100 mW cm^{-2} calibrated with a standard silicon solar cell, Newport, Oriel Class A, 91195A) in a voltage range of 0-1.7 V. The steady power output curves at the maximum power point (MPP) bias voltage were recorded by electrochemical workstation of CHI660E. The monochromatic incident photon-to-electron conversion efficiency (IPCE) spectra was obtained using the IPCE suite of Enli Technology Co., Ltd. equipped with standard silicon solar cells as a reference. Electrochemical impedance spectroscopy (EIS) was performed under dark condition in a frequency range from 1 MHz to 0.1 Hz with an amplitude of 10 mV at V_{OC}. The V_{OC} decay curve was measured in open circuit mode by irradiating with 100 mW cm^{-2} light intensity for several seconds and then instantaneously switching off the light. The dark *J-V* curves were characterized at the scanning rate of 10 mV s^{-1} in the voltage range of -1.5 to 1.5 V.

The capacitance-voltage (*C-V*) curves were detected at a frequency of 5 kHz (amplitude of 30 mV) under dark conditions.

DFT calculation: The plane wave DFT calculations were performed using the Vienna Ab initio Simulation Package.[2,3] The projector augmented wave (PAW) was applied,[4] and the generalized gradient approximation (GGA) within the Perdew-Burke-Ernzerhof (PBE) function was employed to describe the electron exchange-correlation effects.[5] The calculation model used was a random distribution of the F, OH, O terminal groups on the Ti_3C_2 surface at a ratio of 44:34:22 in accordance with XPS characterizations (Fig. 2b and S3a). The Monkhorst-Pack grids of 3×3×1 was used for heterojunction optimization and the structure relaxation was applied by a 400 eV cut-off energy. The structures optimization was obtained when the energy difference was less than 10^{-5} eV and the force per atom was less than 0.01 $eV \cdot Å^{-1}$. A vacuum space of 15 Å was employed to eliminate the interaction between the neighboring layers for periodic boundary condition.

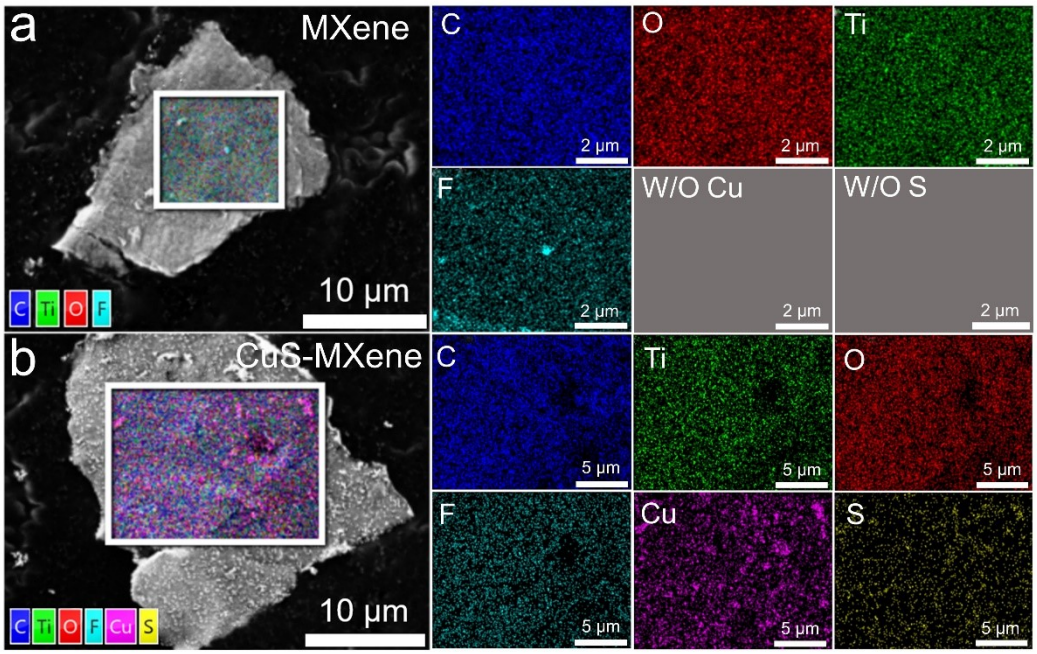

Fig. S1 EDS elemental mapping images of (a) MXene and (b) CuS-MXene nanosheets.

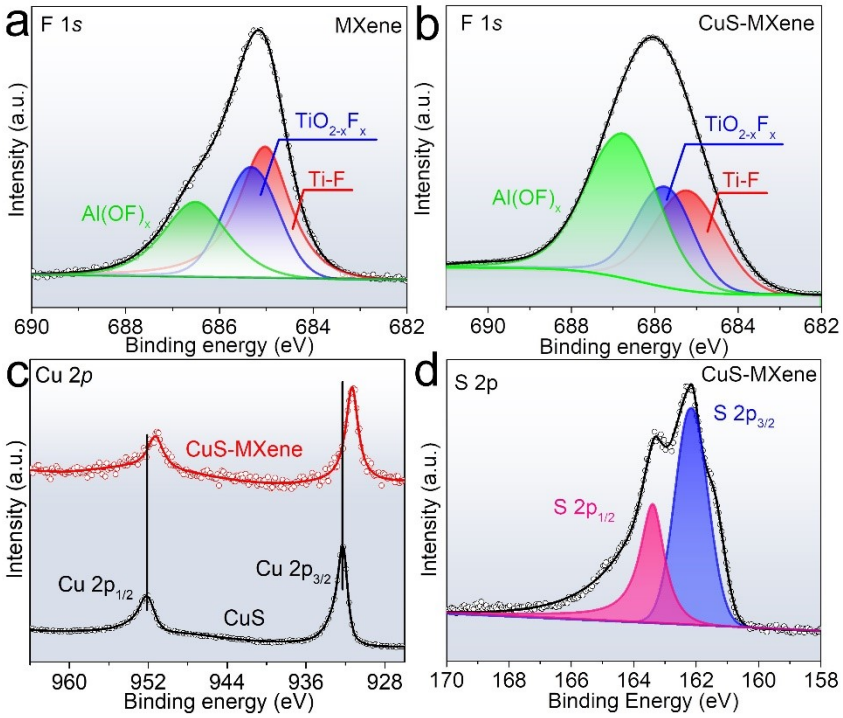

Fig. S2 High-resolution XPS spectra of F 1*s* for (a) MXene and (b) CuS-MXene. (c) High-resolution XPS spectra of Cu 2*p* for CuS and CuS-MXene and (d) S 2*p* for CuS-MXene.

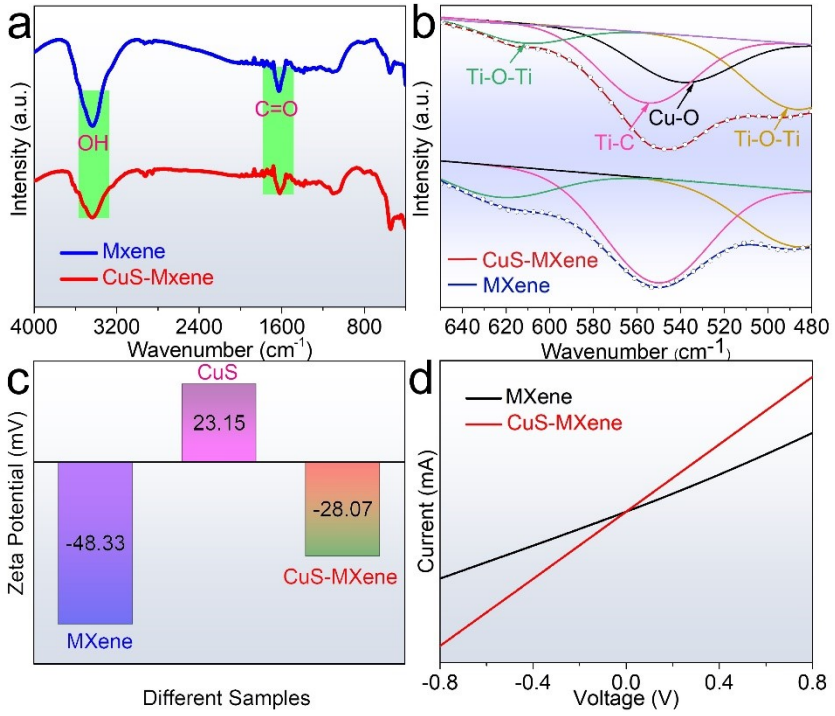

Fig. S3 (a) FT-IR spectra of MXene and CuS-MXene. (b) Gaussian curve fitting of FT-IR for MXene and CuS-MXene. (c) Zeta potentials of CuS, MXene and CuS-MXene. (d) *J-V* curves of the devices with a structure of FTO/MXene or CuS-MXene/Carbon.

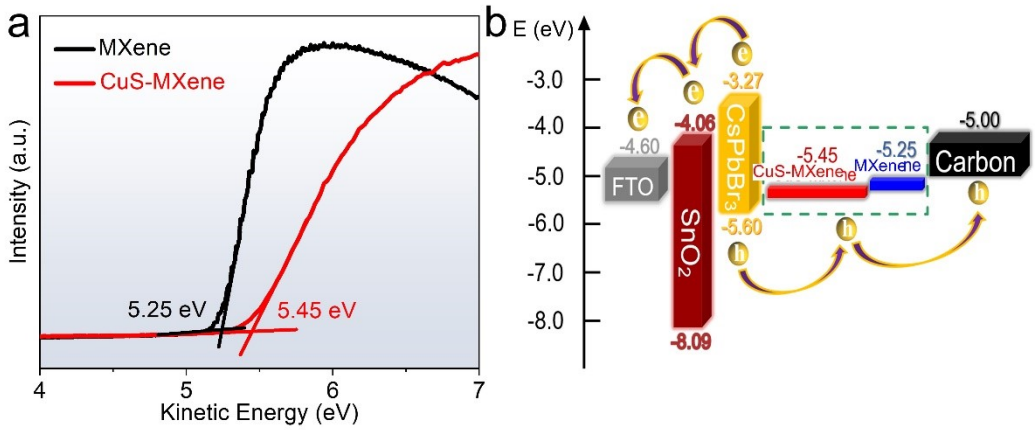

Fig. S4 (a) UPS spectra of MXene and CuS-MXene. (b) Energy level diagram of charge transfer progress in $CsPbBr_3$ PSCs.

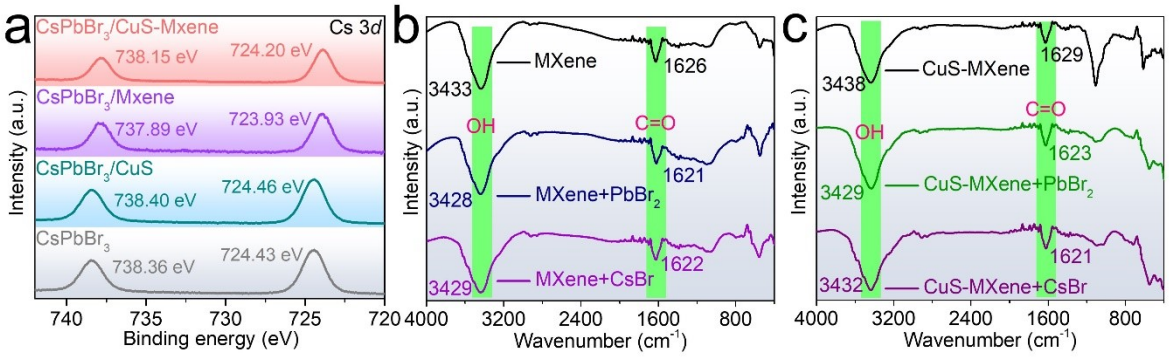

Fig. S5 (a) High-resolution XPS spectra of Cs 3*d* for $CsPbBr_3$, $CsPbBr_3$/CuS, $CsPbBr_3$/MXene and $CsPbBr_3$/CuS-MXene. FT-IR spectra of (b) MXene, MXene+$PbBr_2$ and MXene+CsBr, (c) CuS-MXene, CuS-MXene+$PbBr_2$ and CuS-MXene+CsBr.

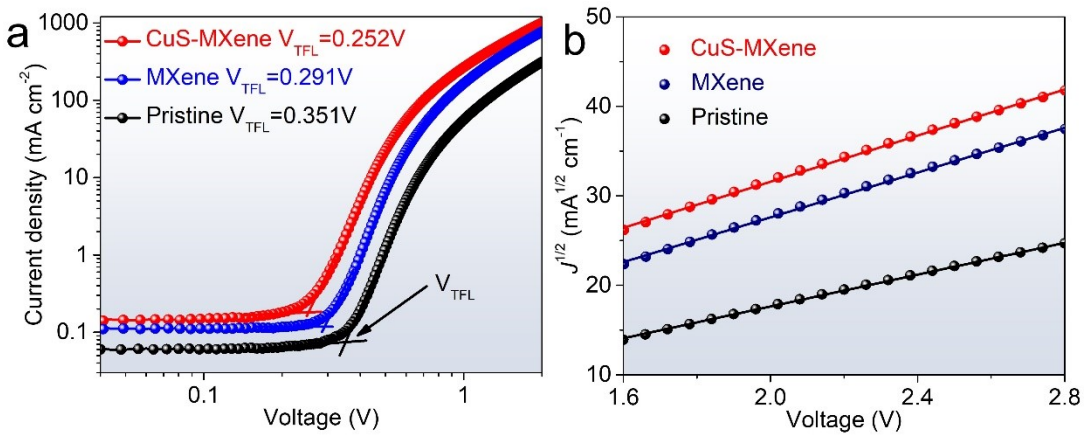

Fig. S6 (a) The *J*-*V* and (b) $J^{1/2}$-*V* curves of devices with a structure of FTO/NiO/$CsPbBr_3$/with and without HTMs/Carbon in dark.

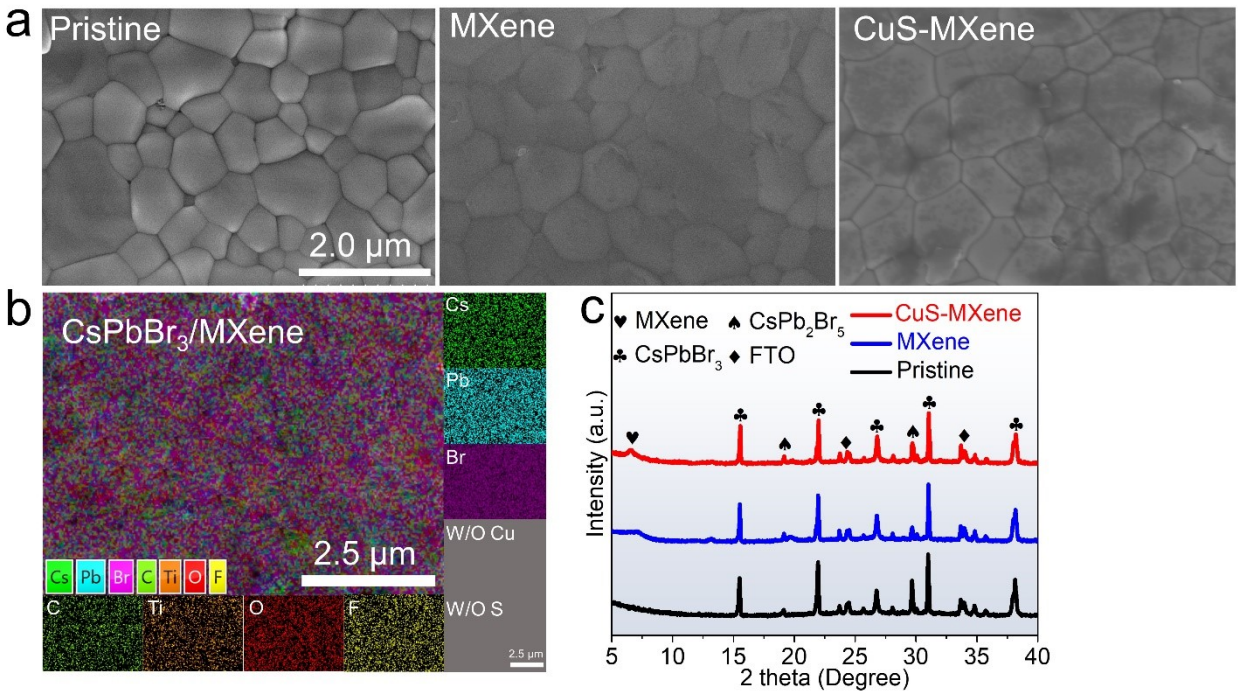

Fig. S7 (a) Top-view SEM images of $CsPbBr_3$, $CsPbBr_3$/MXene and $CsPbBr_3$/CuS-MXene films. (b) EDS elemental mapping images of $CsPbBr_3$/MXene film. (c) XRD patterns of $CsPbBr_3$, $CsPbBr_3$/MXene and $CsPbBr_3$/CuS-MXene films.

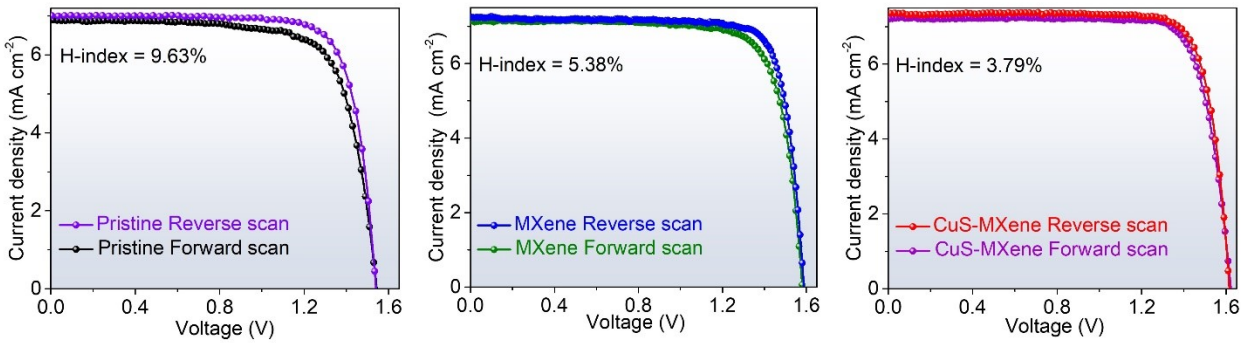

Fig. S8 The *J-V* curves in the reverse and forward scan directions of various $CsPbBr_3$ PSCs. Hysteresis index (H-index) = $(PCE_{reverse} - PCE_{forward}) / PCE_{reverse} \times 100\%$.

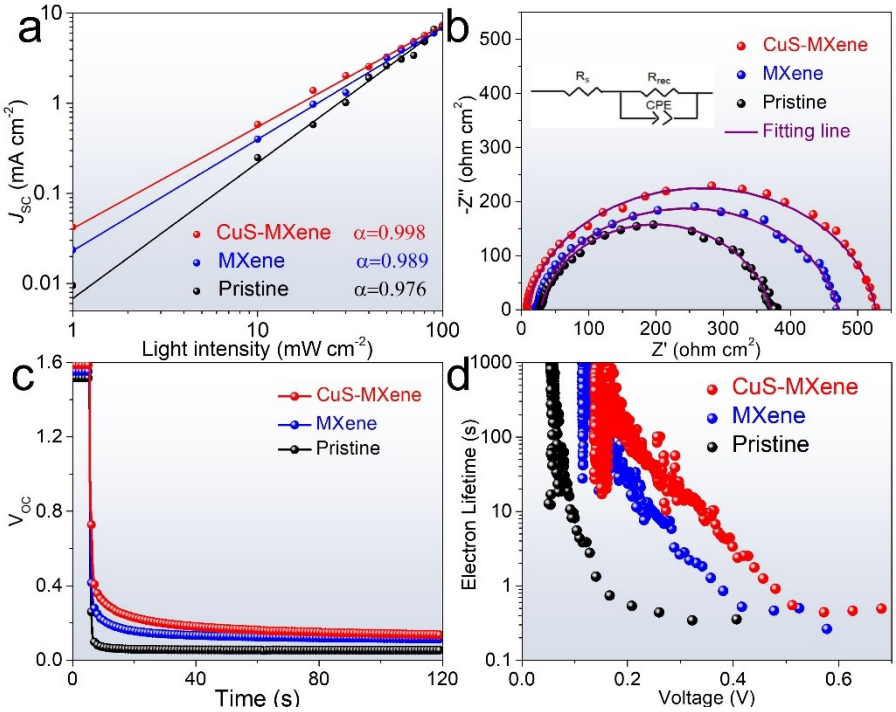

Fig. S9 (a) J_{SC} dependence on light intensity, (b) Nyquist plots, (c) V_{OC} decay curves and (d) electron lifetime of various $CsPbBr_3$ PSCs.

(a) The J_{SC} and I follow a power law dependence according to the equation: $J_{SC} = I^{\alpha} (\alpha \leq 1)$, where α is a factor related to the degree of bimolecular recombination, an α close to 1.0 means a negligible bimolecular recombination.[6]

(b) The EIS spectra is fitted in accordance with the inserted equivalent circuit. The equivalent circuit consists of two parts, one is the series resistance (R_s) of the whole PSCs corresponding to the starting point of the Nyquist plots, while the other is the charge recombination resistance (R_{rec}) within the device corresponding to the circular arc.[7]

(d) The electron lifetime (τ_n) is calculated from V_{OC} decay curves by the formula: $\tau_n = -(k_B T/e)(dV_{OC}/dt)^{-1}$, where k_B and T are the Boltzmann constant and absolute temperature, respectively.[8]

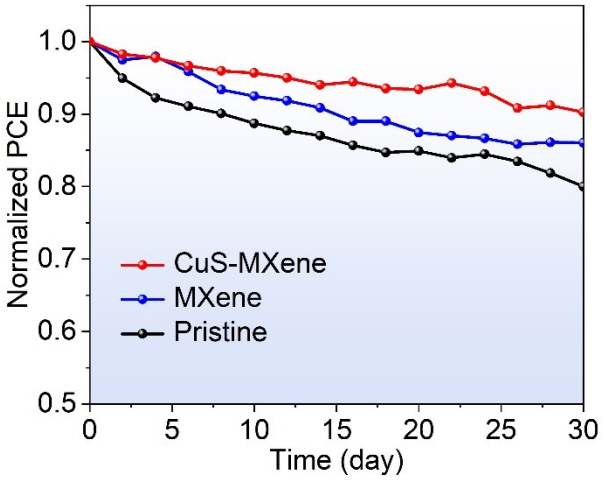

Fig. S10 Long-term stability of various $CsPbBr_3$ PSCs free of encapsulation in air environment with 0% *RH* at 85 °C.

Table S1. The V_{TFL}, n_{trap} and μ_h values of various $CsPbBr_3$ samples.

Samples	V_{TFL} (V)	n_{trap} (10^{15} cm^{-3})	μ_h (10^{-3} cm^2 V^{-1} s^{-1})
Pristine	0.351	4.412	3.455
MXene	0.291	3.658	4.865
CuS-MXene	0.252	3.168	5.013

V_{TFL}: trap-filled limit voltage. n_{trap}: trap state density. μ_h: hole mobility.

The n_{trap} can be calculated from the formula: $n_{trap} = 2\varepsilon\varepsilon_0 V_{TFL}/qL^2$, where L, ε, ε_0 and q are the thickness of the perovskite films, the relative dielectric constant of $CsPbBr_3$, the vacuum permittivity and the elementary charge, respectively. The μ_h can be obtained through the Mott-Gurney law: $\mu_h = 8J_D L^3/9\varepsilon\varepsilon_0 V^2$, where J_D and V refer to the dark current and the applied voltage, respectively.[9]

Table S2. Summary of the photovoltaic parameters of $CsPbBr_3$ PSCs with champion PCE.

Cell configuration	V_{OC} (V)	J_{SC} (mA cm^2)	FF (%)	PCE (%)	Ref
FTO/SnO_2/$CsPbBr_3$/CuS-MXene/Carbon	**1.629**	**7.76**	**83.14**	**10.51**	**This work**
FTO/SnO_2-MCl/$CsPbBr_3$/Carbon	1.601	7.69	81.60	10.04	1
FTO/Sb-TiO_2/$CsPbBr_3$/Carbon	1.654	6.70	80.40	8.91	8
FTO/TiO_2/$CsPbBr_3$/MXene/Carbon	1.444	8.54	73.08	9.01	10
FTO/SnO_2-SnS_2/$CsPbBr_3$/Carbon	1.635	7.80	84.04	10.72	11
FTO/c-TiO_2/m-TiO_2/GQDs/$CsPbBr_3$/Carbon	1.458	8.12	82.10	9.72	12
FTO/c-TiO_2/m-TiO_2/$CsPbBr_3$/P1Z1/Carbon	1.578	7.65	83.10	10.03	13
FTO/c-TiO_2/m-TiO_2/$CsPbBr_3$/ Carbon	1.220	7.40	84.10	7.37	14
FTO/TiO_2/$CsPbBr_3$/SiQDs/spiro-OMeTAD/Ag	1.420	7.80	75.00	8.31	15
ITO/SnO_2/$CsPbBr_3$/spiro-OMeTAD/Au	1.260	10.33	75.30	9.81	16
TiO_2/$CsPbBr_3$/Cu(Cr,Ba)O_2 NCs/Carbon	1.620	7.81	85.50	10.79	17
FTO/TiO_2/$CsPbBr_3$/MnS/Carbon	1.520	8.28	83.00	10.45	18
FTO/TiO_2/PTI-$CsPbBr_3$/spiro-OMeTAD/Ag	1.490	9.78	74.47	10.91	19
FTO/c-TiO_2/$CsPbBr_3$/$CsPbBr_3$-$CsPb_2Br_5$/$CsPbBr_3$–Cs_4PbBr_6/Carbon	1.461	9.24	75.39	10.17	20
FTO/SnO_2-TiO_xCl_{4-2x}/$CsPbBr_3$/Carbon	1.571	7.60	79.60	9.50	21
FTO/TiO_2-AC/$CsPbBr_3$/ZnPc/Carbon	1.606	7.64	82.47	10.12	22
FTO/c-TiO_2/m-TiO_2/$CsPbBr_3$/[BMMIm]Cl/Carbon	1.610	7.45	83.00	9.92	23

FTO/L-TiO_2:$MoSe_2$/$CsPbBr_3$/Carbon	1.615	6.70	78.70	10.02	24
FTO/c-TiO_2/m-TiO_2/Sm^{3+}-$CsPbBr_3$/Carbon	1.594	7.48	85.10	10.14	25
FTO/c-TiO_2/m-TiO2/Sr^{3+}-$CsPbBr_3$/Carbon	1.540	7.71	81.10	9.63	26
FTO/c-TiO_2/ $CsPbBr_3$/spiro-OMeTAD/Au	1.500	5.60	62.00	5.40	27
ITO/ZnO/$CsPbBr_3$/spiro-OMeTAD/Au	1.380	6.15	70.51	5.98	28
FTO/TiO_2/CQD-$CsPbBr_3$IO/spiro-OMeTAD/Au	1.060	11.34	69.00	8.29	29
FTO/c-TiO_2/SnO_2/$CsPbBr_3$/CuPc/Carbon	1.310	8.24	81.40	8.79	30
FTO/c-TiO_2/m-TiO_2/Sn^{2+}-$CsPbBr_3$/Carbon	1.370	7.66	82.22	8.63	31
FTO/c-TiO_2/m-TiO_2/m-ZrO_2/$CsPbBr_3$/m-Carbon	1.440	7.75	73.52	8.20	32
FTO/c-TiO_2/$CsPbBr_3$-$CsPb_2Br_5$/spiro-OMeTAD/Ag	1.296	8.48	75.90	8.34	33
FTO/Fe_2O_3@SnO_2/$CsPbBr_3$/Carbon	1.606	7.88	80.85	10.23	34
FTO/Ga(5%)-SnO_X/$CsPbBr_3$/Carbon	1.336	8.49	71.73	8.13	35
FTO/N-TiO_2/$CsPbBr_3$/Carbon	1.58	6.55	81.96	8.50	36
FTO/TiO_2-ASF/$CsPbBr_3$/Carbon	1.615	7.47	83.56	10.08	37
FTO/TiO_2/$CsPbBr_3$(Cl)/Spiro-OMeTAD/Ag	1.02	8.47	71.60	6.21	38
FTO/TiO_2/$CsPbBr_3$/CZTs/Spiro-OMETAD/Ag	1.12	7.04	68.00	5.36	39
FTO/c-TiO_2/m-TiO_2/$CsPbBr_3$/CZTS/Ag	0.94	7.36	70.01	4.84	40

Table S3. The carrier lifetimes obtained from TRRL spectra of various $CsPbBr_3$ samples.

Samples	τ_{ave} (ns)	τ_1 (ns)	A_1 (%)	τ_2 (ns)	A_2 (%)
Pristine	2.41	0.32	12.74	67.03	87.26
MXene	0.65	0.16	24.30	97.73	75.70
CuS-MXene	0.22	0.15	68.22	17.6	31.78

The TRPL spectra can be fitted by the biexponential decay equation: $I = A_1 e^{-(\tau - \tau_0)\tau_1} + A_2 e^{-(\tau - \tau_0)\tau_2}$, where I is the photoluminescence intensity, A_1 and A_2 are the decay constants, τ_1 and τ_2 are assigned to the trap-induced nonradiative recombination and radiative recombination, respectively. In addition, the average lifetime (τ_{ave}) can be obtained by the following formula: $\tau_{ave} = (A_1\tau_1^2 + A_2\tau_2^2)/(A_1\tau_1 + A_2\tau_2)$.[41]

Table S4. Specific EIS parameters of various $CsPbBr_3$ PSCs.

Samples	R_s (Ω cm^2)	R_{rec} (Ω cm^2)
Pristine	30.84	339.63
MXene	18.93	449.96
CuS-MXene	7.65	518.91

References

1. G. Xie, X. Lu, J. Duan, Y. Dong, X. Jiang, F. Tu, Y. Duan and Q. Tang, *J. Mater. Chem. A*, 2021, **9**, 15003-15011.
2. G. Kresse and J. Furthmuller, *Comput. Mater. Sci*, 1996, **6**, 15-50.
3. G. Kresse and J. Furthmuller, *Phys. Rev. B*, 1996, **54**, 11169-11186.
4. G. Kresse and D. Joubert, *Phys. Rev. B*, 1999, **59**, 1758-1775.
5. J. P. Perdew, K. Burke and M. Ernzerhof, *Phys. Rev. Lett.*, 1996, **77**, 3865-3868.
6. Q. Lou, Y. Han, C. Liu, K. Zheng, J. Zhang, X. Chen, Q. Du, C. Chen and Z. Ge, *Adv. Energy Mater.*, 2021, **11,** 2101416-2101425.
7. Y. Wang, T. Li, Z. Li, S. Wang and X. Deng, *Adv. Funct. Mater.*, 2019, **29,** 1903330-1903338.
8. Y. Xu, J. Duan, X. Yang, J. Du, Y. Wang, Y. Duan and Q. Tang, *J. Mater. Chem. A*, 2020, **8**, 11859-11866.
9. S.-H. Lee, S. Jeong, S. Seo, H. Shin, C. Ma and N.-G. Park, *ACS Energy Lett.*, 2021, **6**, 1612-1621.
10. T. Chen, G. Tong, E. Xu, H. Li, P. Li, Z. Zhu, J. Tang, Y. Qi and Y. Jiang, *J. Mater. Chem. A*, 2019, **7**, 20597-20603.
11. X. Yao, B. He, J. Zhu, J. Ti, L. Cui, R. Tui, M. Wei, H. Chen, J. Duan, Y. Duan and Q. Tang, *Nano Energy*, 2022, **96,** 107138-107145.
12. J. Duan, Y. Zhao, B. He and Q. Tang, *Angew. Chem., Int. Ed.*, 2018, **57**, 3787-3791.
13. Y. Liu, B. He, J. Duan, Y. Zhao, Y. Ding, M. Tang, H. Chen and Q. Tang, *J. Mater. Chem. A*,

2019, **7**, 12635-12644.

14. D. Huang, P. Xie, Z. Pan, H. Rao and X. Zhong, *J. Mater. Chem. A*, 2019, **7**, 22420-22428.
15. S. Zhou, R. Tang, H. Li, L. Fu, B. Li and L. Yin, *J. Power Sources*, 2019, **439,** 227065-227072.
16. P. Wang, X. Zhang, Y. Zhou, Q. Jiang, Q. Ye, Z. Chu, X. Li, X. Yang, Z. Yin and J. You, *Nat. Commun.*, 2018, **9,** 2225-2231.
17. J. Duan, Y. Zhao, Y. Wang, X. Yang and Q. Tang, *Angew. Chem., Int. Ed.*, 2019, **58**, 16147-16151.
18. X. Li, Y. Tan, H. Lai, S. Li, Y. Chen, S. Li, P. Xu and J. Yang, *ACS Appl. Mater. Interfaces*, 2019, **11**, 29746-29752.
19. G. Tong, T. Chen, H. Li, L. Qiu, Z. Liu, Y. Dang, W. Song, L. K. Ono, Y. Jiang and Y. Qi, *Nano Energy*, 2019, **65,** 104015-104024.
20. G. Tong, T. Chen, H. Li, W. Song, Y. Chang, J. Liu, L. Yu, J. Xu, Y. Qi and Y. Jiang, *Sol. RRL*, 2019, **3,** 1900030-1900038.
21. Q. Zhou, J. Duan, Y. Wang, X. Yang and Q. Tang, *J. Energy Chem.*, 2020, **50**, 1-8.
22. J. Zhu, M. Tang, B. He, W. Zhang, X. Li, Z. Gong, H. Chen, Y. Duan and Q. Tang, *J. Mater. Chem. A*, 2020, **8**, 20987-20997.
23. H. Li, G. Tong, T. Chen, H. Zhu, G. Li, Y. Chang, L. Wang and Y. Jiang, *J. Mater. Chem. A*, 2018, **6**, 14255-14261.
24. Q. Zhou, J. Du, J. Duan, Y. Wang, X. Yang, Y. Duan and Q. Tang, *J. Mater. Chem. A*, 2020, **8**, 7784-7791.

25. J. Duan, Y. Zhao, X. Yang, Y. Wang, B. He and Q. Tang, *Adv. Energy Mater.*, 2018, **8,** 1802346-1802354.

26. Y. Zhao, Y. Wang, J. Duan, X. Yang and Q. Tang, *J. Mater. Chem. A*, 2019, **7**, 6877-6882.

27. Q. A. Akkerman, M. Gandini, F. Di Stasio, P. Rastogi, F. Palazon, G. Bertoni, J. M. Ball, M. Prato, A. Petrozza and L. Manna, *Nat. Energy*, 2017, **2,** 16194-16200.

28. W. Chen, J. Zhang, G. Xu, R. Xue, Y. Li, Y. Zhou, J. Hou and Y. Li, *Adv. Mater.*, 2018, **30,** 1800855-1800864.

29. S. Zhou, R. Tang and L. Yin, *Adv. Mater.*, 2017, **29,** 1703682-1703690.

30. X. Liu, X. Tan, Z. Liu, H. Ye, B. Sun, T. Shi, Z. Tang and G. Liao, *Nano Energy*, 2019, **56**, 184-195.

31. H. Guo, Y. Pei, J. Zhang, C. Cai, K. Zhou and Y. Zhu, *J. Mater. Chem. C*, 2019, **7**, 11234-11243.

32. I. Poli, J. Baker, J. McGettrick, F. De Rossi, S. Eslava, T. Watson and P. J. Cameron, *J. Mater. Chem. A*, 2018, **6**, 18677-18686.

33. F. Li, J. Yuan, X. Ling, Y. Zhang, Y. Yang, S. H. Cheung, C. H. Y. Ho, X. Gao and W. Ma, *Adv. Funct. Mater.*, 2018, **28,** 18677-18686.

34. R. Tui, H. Sui, J. Mao, X. Sun, H. Chen, Y. Duan, P. Yang, Q. Tang and B. He, J. *Colloid Interface Sci*., 2023, **640**, 918-927.

35. Y. Zhao, Q. Deng, R. Guo, Z. Wu, Y. Li, Y. Duan, Y. Shen, W. Zhang and G. Shao, *ACS Appl. Mater. Interfaces*, 2020, **12**, 54904-54915.

36. M. Wang, J. Duan, J. Du, X. Yang, Y. Duan, T. Zhang and Q. Tang, *ACS Appl. Mater.*

Interfaces, 2021, **13**, 12091-12098.

37. L. Cui, B. He, Y. Ding, J. Zhu, X. Yao, J. Ti, H. Chen, Y. Duan and Q. Tang, *Chem. Eng. J.*, 2022, **431**, 134193-134201.
38. B. Li, Y. Zhang, L. Zhang and L. Yin, *J. Power Sources*, 2017, **360**, 11-20.
39. Z.-J. Zhou, Y.-Q. Deng, P.-P. Zhang, D.-X. Kou, W.-H. Zhou, Y.-N. Meng, S.-J. Yuan and S.-X. Wu, *Sol. RRL*, 2019, **3**, 1800354-1800359.
40. Z.-J. Zhou, Y.-Q. Deng, P.-P. Zhang, D.-X. Kou, W.-H. Zhou, Y.-N. Meng, S.-J. Yuan and S.-X. Wu, *Sol. RRL*, 2019, **3,** 1800354-1800359.
41. W. Zhang, X. Liu, B. He, Z. Gong, J. Zhu, Y. Ding, H. Chen and Q. Tang, *ACS Appl. Mater. Interfaces*, 2020, **12**, 4540-4548.